RSC Advances

PAPER

View Article Online
View Journal | View Issue

Cite this: *RSC Adv.*, 2019, **9**, 19031

Investigation of the agglomeration reduction mechanism of the aluminized HTPB propellant containing ferric perfluorooctanoate [$Fe(PFO)_3$]†

Fei Zhen,[a] Xuyuan Zhou,[ab] Meishuai Zou,[b] Lingchao Meng,[b] Rongjie Yang,*[a] Liqiong Wang,*[a] Fenglei Huang[a] and Jianmin Li[b]

In this study, ferric perfluorooctanoate [$Fe(PFO)_3$] was used in the aluminized HTPB propellant to reduce Al agglomeration during solid propellant combustion, and the agglomeration reduction mechanism was experimentally demonstrated *via* the burning rate measurement, heat of explosion and Al agglomeration analysis. The behavior of the burning particles on the burning surface as well as the morphology and composition of the quenched burning particles were characterized by microscopic high-speed photography and X-ray photoelectron spectroscopy, respectively; the thermal decomposition properties and gaseous decomposition products of $Fe(PFO)_3$ were investigated by thermal gravimetry-differential scanning calorimetry joint analysis (TG-DSC), Fourier transform infrared spectroscopy (FTIR) and mass spectrometry (MS). The results show that $Fe(PFO)_3$ can significantly increase the burning rate of the aluminized HTPB propellant and reduce Al agglomeration. The aluminized HTPB propellant containing $Fe(PFO)_3$ exhibited a more efficient aluminum combustion process and smaller solid combustion product generation; the agglomeration reduction mechanism was revealed by the comprehensive effects of $Fe(PFO)_3$ on the thermal decomposition of AP and promotion of the thermite reaction with aluminum. It led to the special "immediate detachment upon ignition" phenomenon of Al particles in the propellant and caused the generation of smaller detached burning Al particles. The highly reactive gaseous decomposition products of $Fe(PFO)_3$ could reduce the accumulation of the generated Al_2O_3 on the burning Al particles.

Received 30th March 2019
Accepted 3rd June 2019

DOI: 10.1039/c9ra02393c

rsc.li/rsc-advances

1 Introduction

Metal powder has been widely used as a fuel in solid rocket propellants, and it is one of the most important energy sources in propellants. Some metallic powders, such as aluminum (Al), magnesium (Mg), copper (Cu), iron (Fe) and beryllium (Be), usually have high density and high combustion heat release.[1–3] These advantages have the great potential to make propellants contain more energy. Many engineering studies have proven that the use of a metal fuel is an effective way to increase the specific impulse and combustion flame temperature of the propellant. Therefore, the mass fraction of a metal fuel is required to be increased up to 20% in many current solid propellants.

Because of the advantages of low cost, low oxygen consumption, high density, relatively higher chemical stability and non-toxicity, aluminum powder has been widely used as a metal fuel in composite solid propellants. It has also been proved that the combustion product Al_2O_3 of aluminum can suppress the oscillating combustion in the flow field under solid rocket motor conditions.[4] However, propellants containing high contents of Al powder encounter agglomeration, which is a serious problem, causing Al particles to burn slowly after they leave the burning surface. Moreover, it significantly influences the performance of the solid rocket motor.[5–7] The multiphase flow generated by the agglomerates in the solid rocket motor can reduce the nozzle efficiency. It has been reported that the formation and retention of Al agglomerates can reduce the specific impulse by 2–10%.[5] In addition, the aluminum powder and its oxide products tend to aggregate during combustion process; this results in the interruption of the burning process of Al, lower combustion efficiency of Al and lower energy release for aluminized solid rocket propellants. In addition, high-temperature condensed phase products in the combustion chamber and the nozzle throat can possibly destroy the internal insulation layer of the rocket motor during high-speed motion and cause serious ablation of the nozzle or even blockage of the nozzle throat.[8,9] These defects limit the application of the propellants containing high contents of Al powder.

[a]*State Key Laboratory of Explosion Science and Technology, Beijing Institute of Technology, Zhongguancun South Street No. 5, Beijing 100081, P. R. China. E-mail: wlq2018@sina.com; yrj@bit.edu.cn*

[b]*School of Materials Science and Engineering, Beijing Institute of Technology, Zhongguancun South Street No. 5, Beijing 100081, P. R. China*

† Electronic supplementary information (ESI) available. See DOI: 10.1039/c9ra02393c

A number of studies have been carried out by researchers all over the world to solve the problem of Al agglomeration. The most common solution is the optimization of the mass ratio and size composition of the solid components in propellant formulations. It is aimed at providing better "pocket" parameters based on the classic packing model (or "pocket model"), which has been suggested by Cohen *et al.*[10–13] In addition, some approaches involving the addition of chemical species were considered. Sippel *et al.*[14] have supported that the addition of an appropriate additive (such as polyene or LDPE) with low density is beneficial for the inhibition of Al agglomeration due to its easy gasification. Yagodnikov[15] and Glotov[16] have suggested that the Al agglomeration problem can be solved by adding an organic fluoride to propellant formulations. Zamkov[17] and Koch[18,19] have also reported an application of organic fluorides in energetic materials. Most organic fluorides and their decomposition products have high chemical reactivity. They can react with aluminum powder, producing aluminum fluoride, whose boiling point is obviously lower than the melting point of aluminum oxide. This property is expected to enhance the gasification property of the combustion product and inhibit the agglomeration to a higher extent.

In previously reported studies,[20,21] the synthetized micro–nano ferric perfluorooctanoate $Fe(PFO)_3$ has been reported to be a good ammonium perchlorate (AP) decomposition catalyst. It has also been revealed that $Fe(PFO)_3$ has high chemical reactivity of triggering the thermite reaction at temperture below the melting point of aluminum (660 °C) according to its application research in aluminized composite solid propellant. $Fe(PFO)_3$ is regarded as an effective and potential promoter for the reduction of Al agglomeration in aluminized composite propellants. Based on these accomplished studies, herein, we investigated the feasibility of employing ferric perfluorooctanoate $Fe(PFO)_3$ as a combustion promoter in aluminized composite solid propellants and further discussed its effects on the propellant. The mechanism of the Al agglomeration reduction has also been presented.

2 Experimental

2.1 Preparation of propellant samples

Hydroxyl terminated polybutadiene (HTPB, prepolymer), binder containing plasticizer (DOS, diisooctyl sebacate) and the curing agent diisocyanate for the binder system were supplied by Liming Research Institute of Chemical Industry (China). Moreover, two types of ammonium perchlorate (AP, 5–15 μm and 110–125 μm) were purchased from HuiAn Chemical Industry Co., Ltd. (China). Commercial aluminium powder (4–6 μm) was supplied by Yuanyang Aluminium Industry Co., Ltd., without further modification of Al particles. The required micro–nano $Fe(PFO)_3$ was synthesized according to our previously reported procedure.[20]

The basic formulation (B0) of the HTPB/Al/AP propellant was composed of 18 wt% Al, 67 wt% AP and 15 wt% HTPB binder system. For the formulation containing $Fe(PFO)_3$ (B1), 1.5 wt% AP was substituted by the equivalent mass of $Fe(PFO)_3$. AP/$Fe(PFO)_3$ was first pre-mixed to better disperse $Fe(PFO)_3$ in the HTPB matrix,[22] and the two types of AP particles were also pre-mixed in the mass ratio of 1 : 1 in the formulations to achieve higher propellant density; in addition, the substituted mass of AP was controlled to be less than 3%. That because more $Fe(PFO)_3$ added in propellant would be harmful to the viscosity of propellant processing. After homogeneously mixing all the components, the samples were cured in an incubator for 5–7 days at 60 °C and <30% humidity. The propellant formulations are presented in Table 1. There is no obvious difference between the densities of two formulations.

According to our previous studies,[20,21] the micro–nano $Fe(PFO)_3$ could increase both the decomposition of AP and the reactivity of the aluminium powder. Therefore, in this study, note that $Fe(PFO)_3$ could be regarded as a combustion promoter and not just a burning rate catalyst like some ferric salts used in propellants.

2.2 Characterization

The steady burning rate for different propellant samples was determined by employing a measuring system in a cylindrical high-pressure combustor under 3 MPa and 9 MPa argon;[23] the propellant samples (propellant pellets) with the dimension of 5 mm × 5 mm × 25 mm were ignited by hot-wire igniters in the high-pressure combustor. The average burning rate of the samples would be measured and calculated by the simultaneous length measurement based on the time recording of the burning propellant pellet.

In addition, the heat of explosion of the propellants was determined by the Parr 6200 oxygen bomb calorimeter (Parr Instruments Ltd., USA) under the 3 MPa argon condition. Moreover, the solid combustion products were obtained by an oxygen bomb calorimeter; the particle size distribution of the obtained solid combustion products from the oxygen bomb calorimeter was determined using the Mastersizer-2000 analyzer (Malvern Instruments, Ltd., UK). The scanning electron microscopy (SEM) images of the solid combustion products were acquired by the BCPCAS4800 electron microscope (JEOL, Japan).

To further determine the influence of $Fe(PFO)_3$ on the combustion properties, comprehensively characterize the combustion phenomenon on the burning surface and understand the agglomeration of different formulations, the microscopic high-speed photography was performed to investigate the agglomeration process of the ignited Al particles on the burning surface of the propellants. The microscopic high-speed photography set-up is shown in Fig. 1, which consists of a transparent combustor, a microscopic lens, a high-speed camera and a connected personal computer. The tests were performed at the shooting rate of 4500 frames per second (fps).

Table 1 Propellant formulations

Samples	HTPB binder/wt%	Al/wt%	AP/wt%	$Fe(PFO)_3$/wt%
B0	15	18	67	0
B1	15	18	65.5	1.5

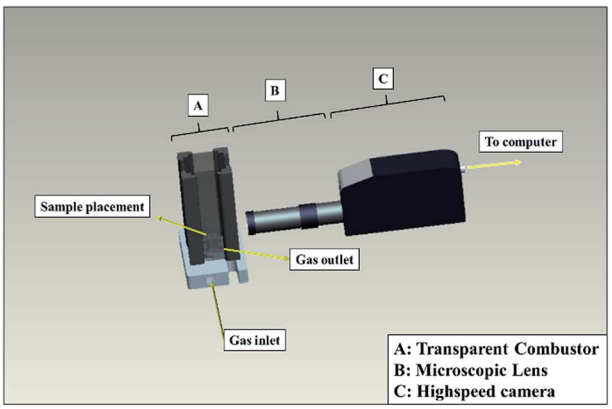

Fig. 1 Schematic of the microscopic high-speed photography set-up.

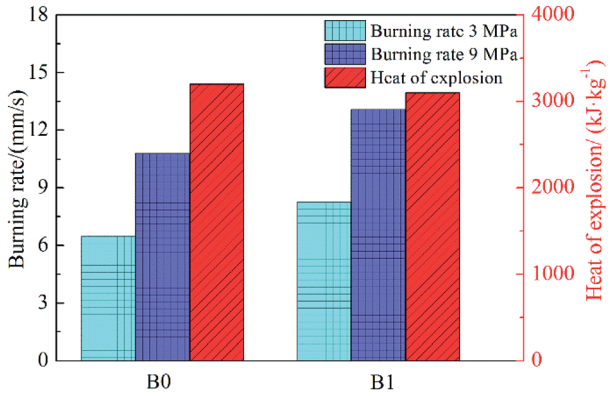

Fig. 3 Comparison of the burning rates and heat of explosion for the propellants B0 and B1.

Moreover, the quenched particles in the combustion flame zone were obtained by a classical quenching technique, as shown in Fig. 2. After being filtered and dried, the quenched particles were analysed by X-ray photoelectron spectroscopy (XPS) using the Quanta II SXM instrument (PHI, Japan). These measurements would provide semi-quantitative information of the interested elements. Size analysis of the quenched particles was also carried out by a statistical method using the SEM images.

To understand the thermal decomposition properties of $Fe(PFO)_3$ and better discuss the combustion mechanism of different propellants, thermal gravimetry (TG), differential scanning calorimetry (DSC), Fourier transform infrared (FTIR) spectroscopy and mass spectrometry (MS) were carried out using a thermal analysis system (STA 449 F3 Jupiter®-Nicolet 6700, Netzsch, Germany).

3 Results and discussion

3.1 Combustion characterization

The combustion and energy properties of the propellants B0 and B1 are presented in Fig. 3. Since the burning rate has been previously investigated in the reported studies,[21] only certain data (under 3 MPa and 9 MPa) are presented herein to illustrate the effect of $Fe(PFO)_3$ on the burning rate of propellants. It increased the burning rate from 6.5 mm s^{-1} (B0) to 8.3 mm s^{-1} (B1) under 3 MPa and from 10.8 mm s^{-1} (B0) to 13.1 mm s^{-1} (B1) under 9 MPa. Therefore, $Fe(PFO)_3$ is regarded as a promoter of the burning rate. Higher pressure would lead to a significant increase in the burning rate for the formulation containing $Fe(PFO)_3$.

The comparison of the heat of explosion for different propellants is plotted in Fig. 3. According to the presented data, the heat of explosion of B0 and B1 is 3258 (±60) kJ kg^{-1} and 3147 (±58) kJ kg^{-1}, respectively. There is a small decrease (~3.4%) in the heat of explosion of the formulation B1 as compared to that of B0. It could be further inferred from our previous study[24] that the theoretical specific impulse of B1 would also exhibit a small decrease based on the tendency of the heat of explosion. Moreover, the decrease in properties may be attributed to the lower oxygen balance in B1.

The solid combustion products (condensed combustion products) of the two propellants were obtained by the oxygen bomb calorimeter under 3 MPa argon. The particle sizes of the solid combustion products were measured to evaluate the agglomeration degree during the combustion process (serious Al agglomeration could generate large combustion products). The distribution curves for the particles of 0.1–200 μm size are plotted in Fig. 4. For better illustration, particles larger than 10

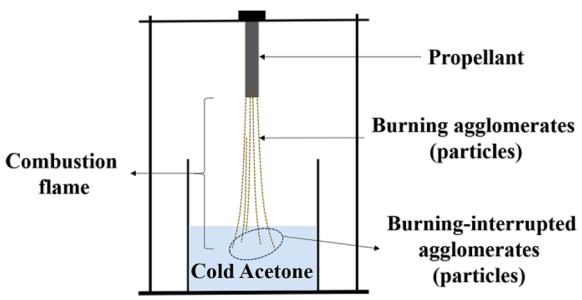

Fig. 2 Schematic of the quenching method.

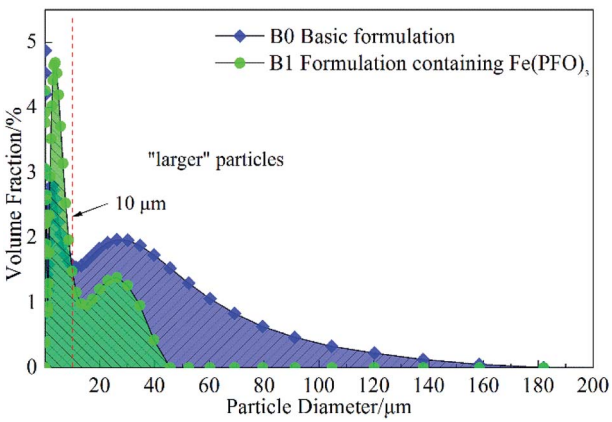

Fig. 4 Comparison of the particle size distribution curves for solid combustion products.

μm were considered "large" particles, and particles smaller than 10 μm were considered "small" particles. The curves indicate the variation of volume fraction in different particle size ranges.

It can be clearly seen that the area of "large" particles in Fig. 4 is obviously reduced with the addition of $Fe(PFO)_3$ to the propellant. The content (volume fraction) of the "large" particles in B1 decreased sharply when compared with that in B0. The particle size of B0 ranges from 0.1 μm to 180 μm, whereas the particle size of B1 exhibits an obviously narrower distribution range from 0.1 μm to 50 μm. This result indicates that the addition of $Fe(PFO)_3$ to the propellant can promote the generation of "small" particles.

SEM images (Fig. 5) demonstrate that there are more well-dispersed particles in the propellant B1 than those in B0. This implies that $Fe(PFO)_3$ can promote the generation of more uniform-sized "small" particles. These findings indicate that during the combustion of the propellant containing $Fe(PFO)_3$, agglomeration can be significantly reduced. The generation of more uniform-sized "small" particles and the reduced agglomeration of Al could infer that there was less mass fraction of active Al in the solid combustion products of the formulation containing $Fe(PFO)_3$, according to our previous study.[24]

3.2 Characterization of the burning particles

To further investigate the agglomeration reduction mechanism of the propellant containing $Fe(PFO)_3$, more detailed information on the burning surface and the burning particles in the combustion flame was achieved. The microscopic high-speed photography was employed to characterize the combustion phenomenon on the burning surface under normal pressure conditions (0.1 MPa). The burning surface characterizations for different formulations are shown in Fig. 6. The time interval between the successive images is about 1.0 ms.

As shown in Fig. 6, the characteristics of the burning surface of the two formulations are significantly different (video records, see Appendix media†). For the basic propellant B0, the burning characteristics of the burning surface are in accordance with those of a normal aluminized propellant during the typical agglomeration process. As marked by the arrow shown in Fig. 6, the ignited Al particles rolled on the burning surface and aggregated to form relatively larger spherical agglomerates. Then, the agglomerates detached from the burning surface and entered the flame zone for further combustion. It is clearly evident from the last image that an agglomerate with a "cap-core" structure was formed from the formulation B0.

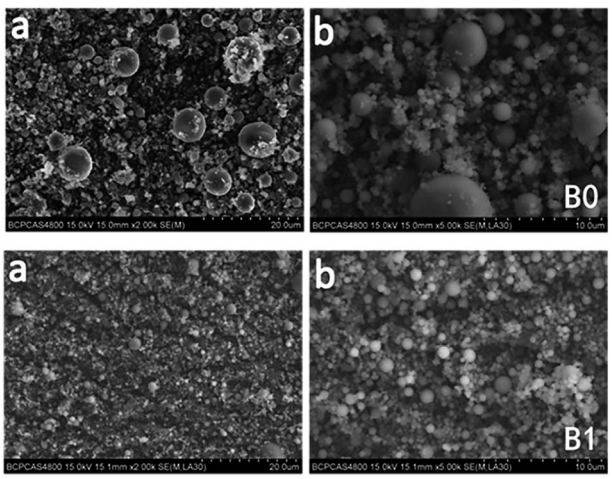

Fig. 5 SEM images with different magnifications ((a) ×2000 and (b) ×5000) of the solid combustion products of two formulations.

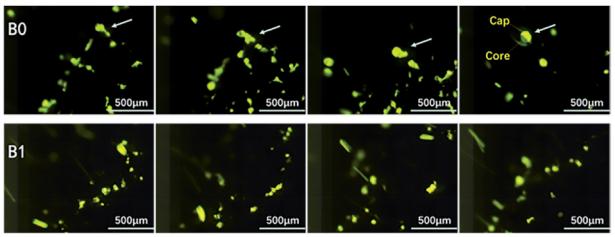

Fig. 6 Combustion characteristics of the burning surfaces of different formulations.

However, the combustion characteristics of the burning surface for the propellant containing $Fe(PFO)_3$ were quite different from those of B0 (Fig. 6). Minor agglomeration was visible in these images, and the ignited Al particles did not aggregate to form homogeneous spherical agglomerates; instead, they tended to splash from the burning surface directly into the flame zone, showing a bright trailing line, known as the "immediate detachment upon ignition" phenomenon. The combustion of the ignited Al particles in B1 was also more violent than that in B0. In addition, some extended and contrastive characterizations were performed on the aluminized HTPB propellant separately containing $Fe(PFO)_3$ and polytetrafluoroethylene powder to compare the effects of $Fe(PFO)_3$ and polytetrafluoroethylene powder on the Al agglomeration process. The related results, including those of the particle size analysis of solid combustion products, the successive images of the combustion process, and the morphology of solid combustion products, are provided in the ESI.†

To understand the burning process, the burning of particles in the flame zone was interrupted, and the particles were captured by the quenching technique (as shown in Fig. 2), which is regarded as a good particle capture method; in this study, cold acetone was used as the quenching medium because its polarity contributes to better preservation of the structure of the quenched particles. The morphological and statistical analysis results of the quenched particles obtained from different formulations are presented in Fig. 7 and 8.

It can be seen in Fig. 7 that both quenched samples consist of spherical particles in the same magnification. The size of the agglomerated particles of B0 ranges from 50 μm to 100 μm, which is much larger than that of B1. Fig. 8 presents the statistical analysis results of the particle size, and the data have been employed to evaluate the agglomeration degree of different formulations. As shown in Fig. 8, for the formulation B0, about 86.4% quenched particles were over 50 μm in size, whereas only 1.7% particles were over 50 μm in the formulation

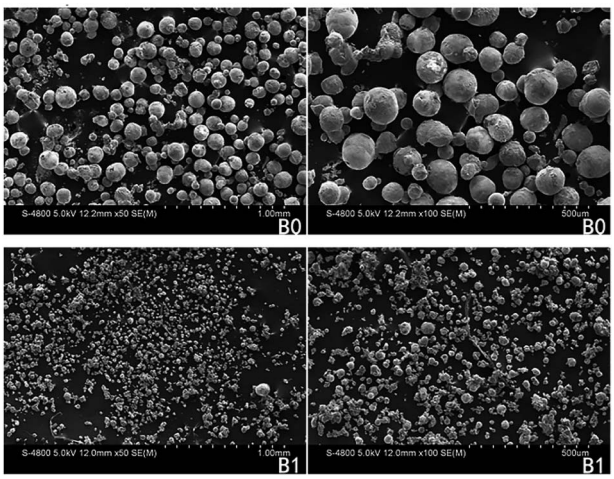

Fig. 7 Morphology images of the quenched burning particles from two formulations.

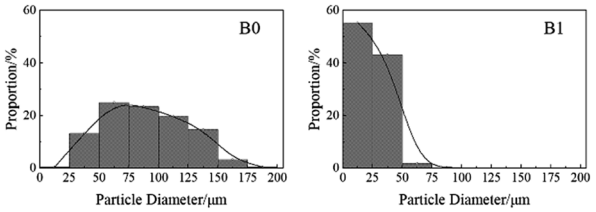

Fig. 8 Statistical analysis results of the quenched burning particles from two formulations.

B1. Due to the formation of these quenched particles by the Al agglomeration process, the Al agglomeration of B0 was more serious than that of B1, namely the agglomeration on the burning surface was well suppressed in the case of B1. This might be attributed to the abovementioned "splash" combustion. The ignited Al particles rapidly detached from the burning surface and easily dispersed in the flame zone, causing the generation of smaller burning particles. These smaller particles foreboded higher combustion efficiency of aluminium.

The quenched particle samples were also analysed by X-ray photoelectron spectroscopy (XPS) to obtain qualitative elemental information, and the corresponding XPS patterns are shown in Fig. 9. It can be seen from the element patterns that the quenched particles of the propellant B0 mainly consist of the elements O and Al, whereas the quenched particles of the propellant B1 consist of the elements O, Al and F; it has been confirmed that some fluoridation occurs on the surface of the burning particles (agglomerates) when the propellant B1 undergoes combustion. *Via* the further analysis of the XPS narrow pattern of Al_{2p}, it was found that the quenched particles from B0 featured only one peak corresponding to aluminium oxide (Al_2O_3) at a high binding energy (B.E. = 74.5 eV). On the other hand, the quenched particles from B1 not only featured one peak corresponding to aluminium oxide (Al_2O_3), but also showed another two special peaks corresponding to the formation of AlF_3 at a high binding energy (B.E. = 75.9 eV) and some unreacted elemental Al at lower binding energy. It was

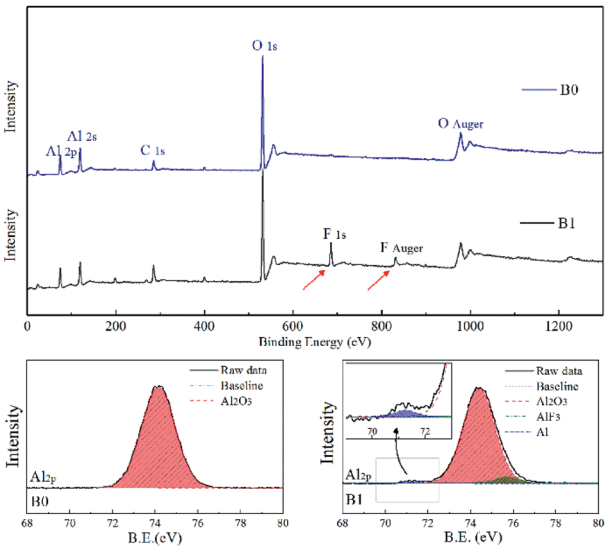

Fig. 9 Element identification and analysis of the Al_{2p} peaks of the quenched burning particles for different formulations.

firmly confirmed that fluoridation occurred on the surface of the burning particles in B1. These results imply that when the particles combust in the propellant containing $Fe(PFO)_3$, AlF_3 simultaneously forms with the formation of Al_2O_3.

Because the depth detected by the XPS equipment is less than 100 nm, XPS data can be regarded as the surface analysis result of the quenched particles. Note that these particles are burning-interrupted aluminium. The burning process of these particles is interrupted by the quenching medium (cold acetone); thus, there must be some unreacted Al inside. For the basic formulation B0, there was no characteristic signal (binding energy) of the unreacted Al, and only the signal of aluminium oxide (Al_2O_3) at the binding energy (B.E.) of 74.5 eV was detected. This occurred because the dense Al_2O_3 generated from the burning aluminium covered the entire quenched particles, and the unreacted Al could only exist in the interior of the quenched particles. For the formulation B1, due to the good gasification property of AlF_3 (boiling point $\sim$ 1800 K), AlF_3 formed on the burning particle surface can easily gasify in the combustion flame zone, in which the temperature usually exceeds 2000 K. Thus, some reactive Al was exposed and detected by the XPS equipment. Thus, a tiny characteristic signal of the unreacted Al at lower binding energy can be seen in Fig. 9.

3.3 Decomposition of $Fe(PFO)_3$

To postulate the agglomeration reduction mechanism, additional analysis of the thermal decomposition properties of $Fe(PFO)_3$ was performed. Moreover, the effect of $Fe(PFO)_3$ on the combustion properties of the propellants was investigated in detail. The thermal gravimetry-differential scanning calorimetry joint analysis (TG-DSC) results are shown in Fig. 10. The Fourier transform infrared spectroscopy (FTIR) and mass spectrometry (MS) analysis results of the gaseous decomposition products of $Fe(PFO)_3$ are presented in Fig. 11.

As shown in the TG-DSC curves in Fig. 10, the decomposition exothermic process of $Fe(PFO)_3$ presents an obvious two-step exothermic decomposition from 250 °C to 400 °C with about 16% residue (solid decomposition products). Because FeF_2, FeF_3, FeO, and Fe_2O_3 have been identified to be catalysis on thermal decomposition of AP,[20] the gaseous decomposition products of $Fe(PFO)_3$ would be also further characterized by FTIR-MS.

The FTIR spectra of the gaseous decomposition products in the range from 250 °C to 400 °C in Fig. 11 show similar reflectance corresponding to the vibrations of hydroxyl (–OH), carbonyl (C=O), fluorocarbon (C–F) and carbon dioxide (CO_2). It is shown that the gaseous decomposition products of $Fe(PFO)_3$ are CO_2 and some carbon fluorides with some oxygen-containing groups. The MS spectrum in the Fig. 11 inset presents the ion fragment ($m/z = 45$) from the carboxyl (–COOH) group and some other fragments of the long-chain fluorocarbon (such as $m/z = 69$, 100, 119, 131, and 181). By integrating both the FTIR and the MS results, it is proved that the gaseous decomposition products of $Fe(PFO)_3$ may be perfluorooctanoic acid, CO_2 and some perfluoro-alkanes.

Furthermore, according to the MS analysis results, the $Fe(PFO)_3$ gaseous decomposition products tend to crack into some fragments containing relatively abundant fluorine such as $^+CF_3$, $^+C_2F_4$ and $^+C_2F_5$ (Fig. 11). According to the reported studies[25–28] on the chemical reactivity of the pyrolysis fragments of polytetrafluoroethylene (PTFE), the fragments with abundant fluorine easily react with alumina and aluminium to form AlF_3 at high temperatures and high heating rate. These results support that the $Fe(PFO)_3$ gaseous decomposition products have high reactivity in the combustion flame of the propellant.

3.4 Discussions on the mechanism of agglomeration reduction

Based on the abovementioned analysis, the gaseous decomposition products of $Fe(PFO)_3$ also have high reactivity (similar to that of PTFE). These gaseous decomposition products can react with Al and Al_2O_3 to form AlF_3. XPS results for quenched burning particles (in Fig. 9) that the existence identification of AlF_3 has confirmed this point. At this point, the agglomeration

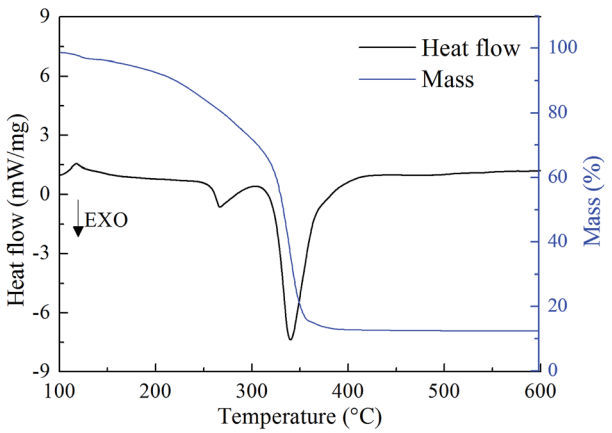

Fig. 10 TG-DSC curve of $Fe(PFO)_3$.

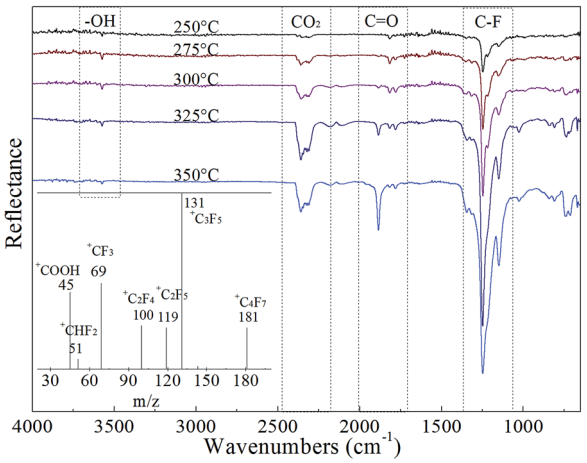

Fig. 11 FTIR and MS analysis results of the $Fe(PFO)_3$ gaseous decomposition products.

reduction mechanism for the aluminized HTPB propellant containing $Fe(PFO)_3$ could be supposed, as shown in Fig. 12.

According to the reported studies,[20,21] $Fe(PFO)_3$ is a good catalyst for the ignition/combustion of the HTPB propellant containing aluminium. It not only catalyses the thermal decomposition of AP but also promotes the thermite reaction with aluminium at low temperatures. This comprehensive effect would increase the gas and heat release from AP and Al, respectively.

The surface residence time of Al particles is determined by the surface force balance, which is influenced by the surface force of the binder skeleton (formed by the decomposing of the HTPB binder), gas flow (mainly determined by the decomposition of AP) and heat release (mainly determined by the decomposition/combustion of AP and ignition/combustion of aluminium). Because the comprehensive effects of $Fe(PFO)_3$ on the thermal decomposition of AP and promotion of the thermite reaction with aluminium are considered to promote faster

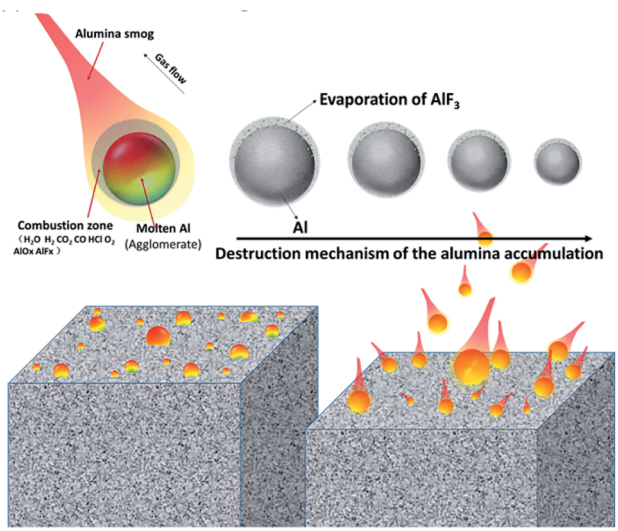

Fig. 12 The proposed mechanism of agglomeration reduction for the aluminized HTPB propellant containing $Fe(PFO)_3$.

gas and heat release from AP and Al, a new surface force balance can be established, which reduces the residence time of Al particles on the burning surface of the propellant. It would result in a special "immediate detachment upon ignition" phenomenon of the Al particles from the propellant; this means that the Al particles would detach from the burning surface immediately after being ignited. This would greatly reduce the residence time of the ignited Al particles on the burning surface to avoid serious aggregation[28] and make the detached burning Al particles for the propellant containing $Fe(PFO)_3$ smaller than those for the basic propellant. It can be confirmed from Fig. 7.

In addition to the result that the detached burning Al particles for the propellant formulation containing $Fe(PFO)_3$ are smaller than those in the case of the basic formulation, the highly reactive $Fe(PFO)_3$'s gaseous decomposition products would further promote the combustion efficiency of the burning Al particles and promote the burning Al particles to form smaller solid combustion products.

Based on the classical combustion model for burning aluminium proposed by Price *et al.*,[29] Al_2O_3 is the final solid combustion product (FSCP). There are two forms of FSCP generated from burning aluminium; one is relatively large sized FSCP, which accumulates on the surface of the burning aluminium. The accumulation of the large-sized FSCP would gradually increase, forming a cap (or a shell, presented in Fig. 6) as the combustion proceeds, covering all the burning particles with just a little unburned aluminium left as an inner core. The other is nano-scale FSCP, which usually disperses with the gas flow (always described as "alumina smog"). Accumulation of the large-sized FSCP is a vital factor for the determination of both the particle diameter and the combustion efficiency of burning aluminium.

In the case of the propellant containing $Fe(PFO)_3$, due to high reactivity of the $Fe(PFO)_3$ gaseous decomposition products, fluoridation of Al and Al_2O_3 would occur on the surface of the burning aluminium with the formation of AlF_3. The low boiling point of AlF_3 endows it with good gasification properties to suppress the accumulation of FSCP, promote its dispersion in the flame zone and form small-sized FSCP. This property would be beneficial to decrease the particle size of the burning aluminium particles and further promote the solid combustion products to be much smaller in the propellant containing $Fe(PFO)_3$, especially considering that the initially burning aluminium particles detached from the propellant containing $Fe(PFO)_3$ are inherently smaller than the basic formulation, as shown in Fig. 7. Moreover, the increased burning rate of the propellant containing $Fe(PFO)_3$ could reduce the Al agglomeration to some degree.[30] Thereby, the particle size of the solid combustion products of the propellant containing $Fe(PFO)_3$ is much smaller than that of the basic formulation, as shown in Fig. 4 and 5.

4 Conclusions

In this study, the particle size analysis of the solid combustion products indicates that the propellant containing 1.5 wt% $Fe(PFO)_3$ can greatly reduce Al agglomeration when compared with the basic propellant without $Fe(PFO)_3$. It is confirmed that the propellant containing $Fe(PFO)_3$ combusts with the splash phenomenon on the burning surface, and some fluoridation (formation of AlF_3) occurs on the surface of the burning aluminium particles. The agglomeration reduction mechanism for the propellant containing $Fe(PFO)_3$ is ascribed to the reactivity of $Fe(PFO)_3$ and its gaseous decomposition products. The comprehensive effects of $Fe(PFO)_3$ on the thermal decomposition of AP and promotion of the thermite reaction with aluminium are considered to lead to a special "immediate detachment upon ignition" phenomenon of Al particles in the propellant. This phenomenon guarantees the generation of smaller detached burning Al particles for the propellant containing $Fe(PFO)_3$. In addition, the formation of easily gasified AlF_3 could suppress the accumulation of Al_2O_3 generated on burning aluminium particles and further stimulate the burning Al particles to form small-sized solid combustion products.

Conflicts of interest

There are no conflicts to declare.

Acknowledgements

We sincerely appreciate the joint thermal analysis support received from Tsinghua University and National Engineering Research Center of Flame Retardant Materials.

References

1 S. Shark, T. R. Sippel, S. Son, S. Heister and T. Pourpoint, *47th AIAA/ASME/SAE/ASEE Joint Propulsion Conference & Exhibit*, 2011.
2 H. Kumar, P. N. Tengli, V. K. Mishra, P. Tripathi, D. B. Pal and P. K. Mishra, *RSC Adv.*, 2017, **7**, 36594.
3 T. F. Zhang, Z. Ma, G. P. Li and Y. J. Luo, *RSC Adv.*, 2017, **7**, 904.
4 L. DeLuca, *International Autumn Seminar on Propellants, Explosives and Pyrotechnics*, 2007, p. 277.
5 T. K Liu, H. C. Perng, S. P Luh and F. Liu, *J. Propul. Power*, 1992, **8**, 1177.
6 V. Rosenband and A. Gany, *Combust. Sci. Technol.*, 2001, **166**, 91.
7 L. Deluca, A. Bandera and F. Maggi, *45th AIAA/SAE/ASEE Joint Propulsion Conference & Exhibit*, 2009, vol. 1.
8 S. A. Rashkovskii, *Combust., Explos. Shock Waves*, 2007, **43**, 654.
9 H. J. Xiang and G. Y. Fang, *J. Propul. Technol.*, 2002, **23**, 366.
10 N. S. Cohen, *AIAA J.*, 1983, **21**, 720.
11 S. P. Luh, T. K. Liu and H. C. Perng, *31th AIAA/SAE/ASEE Joint Propulsion Conference & Exhibit*, 1995, vol. 1.
12 J. C. Mullen and M. Q. Brewster, *J. Propul. Power*, 2011, **27**, 650.
13 R. C. Smith, *J. Spacecr. Rockets*, 1968, **5**, 1360.
14 T. R. Sippel, S. F. Son, L. J. Groven, S. Zhang and E. L. Dreizin, *Combust. Flame*, 2015, **162**, 846.

15 D. A. Yagodnikov, E. A. Andreev, V. S. Vorob'Ev and O. G. Glotov, *Combust., Explos. Shock Waves*, 2006, **42**, 534.
16 O. G. Glotov, D. A. Yagodnikov, V. S. Vorob'Ev, V. E. Zarko and V. N. Simonenko, *Combust., Explos. Shock Waves*, 2007, **43**, 320.
17 M. A. Zamkov, R. W. Conner and D. D. Dlott, *J. Phys. Chem. C*, 2007, **111**, 10278.
18 E. C. Koch, *Propellants, Explos., Pyrotech.*, 2002, **27**, 262.
19 E. C. Koch, *Propellants, Explos., Pyrotech.*, 2004, **29**, 9.
20 P. Tu, M. Zou, R. J. Yang and X. Guo, *Thermochim. Acta*, 2016, **646**, 32.
21 F. Zhen, X. Y. Zhou, L. Q. Wang, R. J. Yang and F. L. Huang, *Propellants, Explos., Pyrotech.*, 2019, **44**, 362.
22 J. Xu, Z. Y. Ma, M. X. Zha and F. Q. Zhao, *Acta Armamentarii*, 2013, **34**, 547.
23 R. J. Yang, Y. P. Li, Y. F. Liu and Z. C. Hua, *J. Propul. Technol.*, 2000, **21**, 86.
24 X. Y. Zhou, M. S. Zou, F. L. Huang, R. J. Yang and X. Y. Guo, *Propellants, Explos., Pyrotech.*, 2017, **42**, 417.
25 M. Losada and S. Chaudhuri, *J. Phys. Chem. A*, 2009, **113**, 5933.
26 M. L. Pantoya and S. W. Dean, *Thermochim. Acta*, 2009, **493**, 109.
27 M. A. Hobosyan, K. G. Kirakosyan, S. L. Kharatyan and K. S. Martirosyan, *J. Therm. Anal. Calorim.*, 2015, **119**, 245.
28 R. W. Hermsen, *19th Aerospace Sciences Meeting*, 1981.
29 J. K. Sambamurthi, E. W. Price and R. K. Sigmant, *AIAA J.*, 1984, **22**, 1132.
30 S. Isert, L. Xin, J. Xie and S. F. Son, *Combust. Flame*, 2017, **183**, 322.